

Mode coupling with Fabry-Perot modes in photonic crystal slabs

Ken Qin(秦恳), Peng Hu(胡鹏), Jie Liu(刘杰), Hong Xiang(向红), and De-Zhuan Han(韩德专)
Citation: Chin. Phys. B, 2024, 33 (**8**): 084205. DOI: 10.1088/1674-1056/ad4ff8

What follows is a list of articles you may be interested in

Tailoring topological corner states in photonic crystals by near- and far-field coupling effects

Zhao-Jian Zhang(张兆健), Zhi-Hao Lan(兰智豪), Huan Chen(陈欢), Yang Yu(于洋), and Jun-Bo Yang(杨俊波)
Chin. Phys. B, 2023, 32 (**12**): 124201. DOI: 10.1088/1674-1056/acddd3

Optomagnonically tunable whispering gallery cavity laser wavelength conversion

Yining Zhu(朱奕宁), Zixu Zhu(朱子虚), Anbang Pei(裴安邦), and Yong-Pan Gao(高永潘)
Chin. Phys. B, 2023, 32 (**2**): 024206. DOI: 10.1088/1674-1056/ac7862

Dynamically tunable multiband plasmon-induced transparency effect based on graphene nanoribbon waveguide coupled with rectangle cavities system

Zi-Hao Zhu(朱子豪), Bo-Yun Wang(王波云), Xiang Yan(闫香), Yang Liu(刘洋), Qing-Dong Zeng(曾庆栋), Tao Wang(王涛), and Hua-Qing Yu(余华清)
Chin. Phys. B, 2022, 31 (**8**): 084210. DOI: 10.1088/1674-1056/ac7e39

Single-mode antiresonant terahertz fiber based on mode coupling between core and cladding

Shuai Sun(孙帅), Wei Shi(史伟), Quan Sheng(盛泉), Shijie Fu(付士杰), Zhongbao Yan(闫忠宝), Shuai Zhang(张帅), Junxiang Zhang(张钧翔), Chaodu Shi(史朝督), Guizhong Zhang(张贵忠), and Jianquan Yao(姚建铨)
Chin. Phys. B, 2021, 30 (**12**): 124205. DOI: 10.1088/1674-1056/ac032e

Fiber core mode leakage induced by refractive index variation in high-power fiber laser

Ping Yan(闫平), Xuejiao Wang(王雪娇), Yusheng Huang(黄昱升), Chen Fu(付晨), Junyi Sun(孙骏逸), Qirong Xiao(肖起榕), Dan Li(李丹), Mali Gong(巩马理)
Chin. Phys. B, 2017, 26 (**3**): 034205. DOI: 10.1088/1674-1056/26/3/034205

RAPID COMMUNICATION

Mode coupling with Fabry–Perot modes in photonic crystal slabs

Ken Qin(秦恳)[1], Peng Hu(胡鹏)[2], Jie Liu(刘杰)[1], Hong Xiang(向红)[1,†], and De-Zhuan Han(韩德专)[1,‡]

[1] *Department of Physics and Chongqing Key Laboratory for Strongly Coupled Physics, Chongqing University, Chongqing* 401331, *China*
[2] *School of Science, Chongqing Key Laboratory of New Energy Storage Materials and Devices, Chongqing University of Technology, Chongqing* 400054, *China*

(Received 13 April 2024; revised manuscript received 22 May 2024; accepted manuscript online 24 May 2024)

Fabry–Perot (FP) modes are a class of fundamental resonances in photonic crystal (PhC) slabs. Owing to their low quality factors, FP modes are frequently considered as background fields with their resonance nature being neglected. Nevertheless, FP modes can play important roles in some phenomena, as exemplified by their coupling with guided resonance (GR) modes to achieve bound states in the continuum (BIC). Here, we further demonstrate the genuine resonance mode capability of FP modes PhC slabs. Firstly, we utilize temporal coupled-mode theory to obtain the transmittance of a PhC slab based on the FP modes. Secondly, we construct exceptional points (EPs) in both momentum and parameter spaces through the coupling of FP and GR modes. Furthermore, we identify a Fermi arc connecting two EPs and discuss the far-field polarization topology. This work elucidates that the widespread FPs in PhC slabs can serve as genuine resonant modes, facilitating the realization of desired functionalities through mode coupling.

Keywords: Fabry–Perot mode, photonic crystal slab, mode coupling, exceptional point

PACS: 42.25.Ja, 42.25.Bs, 78.67.Pt, 78.67.–n **DOI:** 10.1088/1674-1056/ad4ff8

1. Introduction

The Fabry–Perot (FP) mode is a fundamental concept in optics and photonics. It refers to the resonance phenomenon occurring within an optical cavity formed by two parallel reflecting surfaces, such as mirrors.[1] FP modes find wide applications in areas such as laser cavities, interferometry, and optical telecommunications, making them a cornerstone in modern optical science and technology.[2,3] In addition to intentionally designed Fabry–Perot structures with highly reflective mirrors, FP modes are also widely present in planar structures such as photonic crystal (PhC) slabs.[4,5] Another important type of modes in PhC slabs is the guided resonances (GRs),[4] where periodic perturbations cause the original guided mode to transition into leaky modes. Compared with the GR modes, FP modes usually have much lower Q factors and thus can be regarded as background fields.[6–10] However, FP modes can play a significant role in some scenarios. For example, the single resonance parametric bound states in the continuum (BIC)[11,12] can be viewed as arising from the coupling between GR and FP modes, thus it can be classified as a special type of Friedrich–Wintgen BIC.[13]

PhC slabs, due to the fabrication simplicity, designable band structures and abundance of radiation polarization, have attracted much interest in light field manipulation. Compared with photonic crystals with infinite volume, a notable feature of photonic crystal slabs is their tendency to radiate outward, necessitating their description within a non-Hermitian framework. Peculiar phenomena can arise in non-Hermitian systems with no counterpart found in Hermitian frameworks. One such example is the exceptional point (EP), a special type of band singularity at which two or more eigenvalues and the corresponding eigenstates coalesce simultaneously.[2,14,15] When the parameters of the system pass through an EP, the energy spectrum and wave functions of the system undergo drastic changes, which give rise to many interesting phenomena, such as unidirectional invisibility,[16] topological chirality,[17,18] and applications in sensing,[19–21] lasing,[22,23] topological energy transfer[24,25] and polarization manipulation.[26,27] PhC slabs offer abundant resonance modes for mode coupling, thus EPs can be readily achieved on this platform. In the reported works, EPs arise mainly from the coupling of two GRs[28–31] and EPs generated via the coupling of FP modes have not been reported.

In this paper, we focus on the resonance nature of the FP mode and discuss its coupling with electromagnetic (EM) waves. First, we use the temporal coupled-mode theory (TCMT)[32] and transmission matrix method (TMM)[1] to demonstrate the feasibility of treating FP resonances as genuine EM modes in a low-contrast PhC slab, where the transmission results from the coupling of FP modes with the incoming and outgoing waves. Next, we employ the coupling of FP modes and GR modes to construct EPs in PhC slabs. EP pairs and the connecting Fermi arc[33] are observed, and the corresponding far-field polarization topology is discussed. Given widespread occurrence of FP modes in PhC slabs, coupling

†Corresponding author. E-mail: xhong@cqu.edu.cn
‡Corresponding author. E-mail: dzhan@cqu.edu.cn

© 2024 Chinese Physical Society and IOP Publishing Ltd

with FP modes may offer more opportunities for achieving diverse functionalities.

2. Transmission of a PhC slab based on mode coupling with FP modes

For a PhC slab with a low index contrast, the transmission can be directly calculated with TMM[1] based on the effective medium theory.[34] In this method, no resonance modes are involved, even though resonance occurs at the transmission peaks. Consider a one-dimensional PhC slab shown in Fig. 1(a). When the index contrast is low, the PhC slab can be approximated as a uniform slab with an effective dielectric constant, as illustrated in Fig. 1(b). The effective dielectric constant for the transverse electric (TE) mode and transverse magnetic (TM) mode satisfies $\varepsilon_{\rm eff} = \varepsilon_1 f + \varepsilon_2(1-f)$ and $1/\varepsilon_{\rm eff} = f/\varepsilon_1 + (1-f)/\varepsilon_2$, respectively. Here ε_1 and ε_2 are the relative dielectric constants of the constitutive media of the PhC slab, and f is the filling ratio of the medium. In the following, we consider the TE mode.

With the TMM, the field distribution inside and outside of the slab can be calculated and the transmittance is obtained as

$$T = \frac{1}{1+\frac{1}{4}(\eta-\eta^{-1})^2\sin^2(k_{2,z}h)}, \tag{1}$$

where $\eta = k_{2,z}/k_{1,z}$, and $k_{1,z}$, $k_{2,z}$ are the z components of the wave vector outside and inside of the slab, respectively. When $\sin^2 k_{2,z}h = 0$, i.e., $k_{2,z}h = m\pi$ (m is an integer), the transmittance reaches the maximum value of 1, while when $k_{2,z}h = (m+1)\pi$, the transmittance reaches the minimum value.

On the hand, the photonic crystal slab can be regarded as a cavity with multipole FP modes resonating at different frequencies. In this sense, we can analyze the transmission of a dielectric slab using the resonant nature of FP modes in the form of mode coupling. According to TCMT, the transmission behavior can be regarded as follows: the incident light partially transmits directly and partially couples to the FP modes in the slab, and then the FP modes couple to the radiation channel, contributing to the transmission.

As an example, we consider the transmission at normal incidence in the frequency range covering the first two FP modes. The system possesses mirror symmetry and has two radiation channels (upward and downward). The dynamic equations governing the coupling of the two FP modes are given by[32]

$$\mathrm{i}\frac{\mathrm{d}}{\mathrm{d}t}a = Ha + \mathrm{i}K^{\mathrm{T}}S_+, \quad S_- = CS_+ + Da. \tag{2}$$

Here, $H = \Omega - \mathrm{i}\Gamma$, with $\Omega = \begin{bmatrix}\omega_0 & 0\\ 0 & 2\omega_0\end{bmatrix}$ and $\Gamma = \begin{bmatrix}\gamma & 0\\ 0 & \gamma\end{bmatrix}$, is the Hamiltonian, a denotes the amplitude of the two FP modes, ω ($\omega_0 = \pi c/(nd)$) and 2ω are the eigenfrequencies of the first two FP modes, and γ stands for the decay rate of the mode due to coupling to the radiation channels. As the resonance frequencies of the FP modes are evenly spaced, their decay rates are assumed to be the same. Due to the symmetry difference of the two modes, no coupling between the two modes is considered. S_+ and S are the amplitudes of the incoming and outgoing waves; C represents the scattering matrix for the direct (nonresonant) transmission and reflection, K and D are the coupling matrices for the modes to the incoming and outgoing waves, respectively. The matrices above are connected as[32]

$$D^{\dagger}D = 2\Gamma, \quad K = D, \quad CD^{*} = -D. \tag{3}$$

Considering the symmetries of the system and the two FP modes, according to $D^{\dagger}D = 2\Gamma$ we have $D = \sqrt{\gamma}\begin{bmatrix}\mathrm{e}^{\mathrm{i}\alpha} & \mathrm{e}^{\mathrm{i}\beta}\\ \sigma\mathrm{e}^{\mathrm{i}\alpha} & -\sigma\mathrm{e}^{\mathrm{i}\beta}\end{bmatrix}$, where α and β are the phase factors to be determined, and $\sigma = \pm 1$ indicates the symmetries of the two modes (with 1 for mode 1 being symmetric and mode 2 being antisymmetric while -1 for the opposite). As matrix C is unitary and symmetric, according to the third equation in Eq. (3) we have $\alpha + \beta = l\pi$ with l an arbitrary integer. For simplicity, we set $\alpha = -\beta$ and then we obtain $C = -\begin{bmatrix}\cos 2\alpha & \mathrm{i}\sigma\sin 2\alpha\\ \mathrm{i}\sigma\sin 2\alpha & \cos 2\alpha\end{bmatrix}$. Assume that the resonant state behaves as simple harmonic oscillation with frequency ω, we have $a = \mathrm{i}(\omega I - H)^{-1}K^{\mathrm{T}}S_+$. Inserting a into the second equation of Eq. (2), the connection between S_+ and S_- is obtained and can be rewritten as $S_- = C'S_+$, with

$$C' = -\begin{bmatrix}\cos 2\alpha & \mathrm{i}\sigma\sin 2\alpha\\ \mathrm{i}\sigma\sin 2\alpha & \cos 2\alpha\end{bmatrix} + \gamma\begin{bmatrix}\frac{\mathrm{e}^{\mathrm{i}2\alpha}}{\gamma+\mathrm{i}(\omega_0-\omega)} + \frac{\mathrm{e}^{-\mathrm{i}2\alpha}}{\gamma+\mathrm{i}(2\omega_0-\omega)} & \frac{\sigma\mathrm{e}^{\mathrm{i}2\alpha}}{\gamma+\mathrm{i}(\omega_0-\omega)} - \frac{\sigma\mathrm{e}^{-\mathrm{i}2\alpha}}{\gamma+\mathrm{i}(2\omega_0-\omega)}\\ \frac{\sigma\mathrm{e}^{\mathrm{i}2\alpha}}{\gamma+\mathrm{i}(\omega_0-\omega)} - \frac{\sigma\mathrm{e}^{-\mathrm{i}2\alpha}}{\gamma+\mathrm{i}(2\omega_0-\omega)} & \frac{\mathrm{e}^{\mathrm{i}2\alpha}}{\gamma+\mathrm{i}(\omega_0-\omega)} + \frac{\mathrm{e}^{-\mathrm{i}2\alpha}}{\gamma+\mathrm{i}(2\omega_0-\omega)}\end{bmatrix}. \tag{4}$$

On the other hand, the entries of the scattering matrix are connected to the reflection coefficient r and transmission coefficient t as $C' = \begin{bmatrix}r & t\\ t & r\end{bmatrix}$, with $|r|^2 + |t|^2 = 1$ and $r^*t + t^*r = 0$, indicating the unitarity of the scattering matrix. From Eq. (4), we obtain the transmittance of the system T ($= |t|^2$) as $T = \left|-\mathrm{i}\sigma\sin 2\alpha + \sigma\left[\frac{\gamma\mathrm{e}^{\mathrm{i}2\alpha}}{\gamma+\mathrm{i}(\omega_0-\omega)} - \frac{\gamma\mathrm{e}^{-\mathrm{i}2\alpha}}{\gamma+\mathrm{i}(2\omega_0-\omega)}\right]\right|^2$. For the two lowest-order FP modes considered here, $\sigma = -1$ since the first mode is odd and the second one is even. According to the result obtained with the TMM method, T reaches its minimum value at $\omega = (3/2)\omega_0$, we obtain $T_{\min} = \frac{(\sin 2\alpha + 2Q\cos 2\alpha - Q^2\sin 2\alpha)^2}{(1+Q^2)^2}$, where $Q = \omega_0/(2\gamma)$ is the quality factor. At $\omega = \omega$ and 2ω, T reaches its maximum value of 1, thus we obtain $T_{\max} = \frac{(2Q\cos 2\alpha + \sin 2\alpha)^2}{1+4Q^2}$. In this way the values of α and γ can be determined and the transmittance of the system is obtained.

Figure 1(c) illustrates the transmittance of a PhC slab with a low index contrast obtained from TCMT and TMM based on the effective medium approximation. As for comparison, the numerical results based on finite element method are also presented. One can see that the result from TMM coincides with that of the numerical simulation. For TCMT, the result agrees well with that of the TMM, especially in the region between the two transmission peaks, manifesting the effectiveness of the assumption above. However, in the frequency range beyond the two peaks, noticeable discrepancy appears. In this area, other FP modes are involved in the transmittance. To accurately capture the transmittance across a wide frequency range, more FP modes should be incorporated into the couple mode theory.

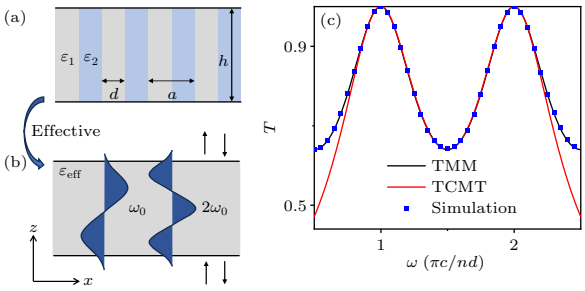


Fig. 1. (a) Depiction of a one-dimensional binary PhC slab, which is characterized by the period a, thickness of one dielectric layer d, slab thickness h, and the relative dielectric constants ε_1 and ε_1. The slab is uniform and infinite in the y-direction. (b) The effective homogeneous medium slab with a relative dielectric constant of ε_{eff}. The field distributions of the two lowest FP modes at frequencies ω_0 and $2\omega_0$ are illustrated schematically. The arrows indicate the incoming and outgoing waves. (c) Transmittance obtained from TMM (black line), TCMT (red line) and numerical simulation (blue dots). Here $\varepsilon_1 = 3.9$, $\varepsilon_2 = 4.1$, $h = a$, $d = 0.5a$.

3. EPs due to the coupling of GR and FP modes

In the non-Hermitian optical system, EPs typically emerge due to the coupling of resonant modes. For example, a second-order EP can be described by the coupled-mode equation[35]

$$\mathrm{i}\frac{\mathrm{d}}{\mathrm{d}t}\begin{bmatrix} a_1 \\ a_2 \end{bmatrix} = \begin{bmatrix} \omega_1 - \mathrm{i}\gamma_1 & \kappa \\ \kappa & \omega_2 - \mathrm{i}\gamma_2 \end{bmatrix}\begin{bmatrix} a_1 \\ a_2 \end{bmatrix}, \tag{5}$$

where a, ω and γ represent the amplitude, resonant frequency and decay rate of the resonant modes, respectively, and κ is the coupling strength. The eigenvalues of the system are

$$\lambda_{\pm} = \omega' - \mathrm{i}\gamma' \pm \sqrt{\kappa^2 + (\omega'' - \mathrm{i}\gamma'')^2}, \tag{6}$$

with $\omega' = (\omega_1 + \omega_2)/2$, $\gamma' = (\gamma_1 + \gamma_2)/2$, $\omega'' = (\omega_1 - \omega_2)/2$, and $\gamma'' = (\gamma_1 - \gamma_2)/2$. When $\kappa^2 + (\omega'' - \mathrm{i}\gamma'')^2 = 0$, two eigenvalues coalesce and an EP is formed.

In the reported works, most EPs arise from the coupling of two GR modes. Here we show that the coupling of FP and GR modes can give rise to EPs as well, and more interestingly, a Fermi arc can be observed.

First, we consider the coupling of the FP and GR modes with the same polarization. For convenience, the two modes are labeled as $\text{FP}_{\text{TM},l}$ and $\text{GR}^{(m)}_{\text{TM},n}$, respectively. Here, l and n represent the order of the FP and GR modes, respectively, and m is the index of band folding in the reduced-zone scheme. We take the coupling of $\text{FP}_{\text{TM},3}$ and $\text{GR}^{(-1)}_{\text{TM},1}$ modes as an example. As the two modes have the same polarization, we consider their coupling along the k_x axis ($k_y = 0$) with the variation of the thickness of the slab. Figures 2(a) and 2(b) show the real and imaginary parts of the eigenvalues of the system in the two-dimensional parameter space (k_x, h), respectively. One can see that the two sheets, for both the real and imaginary parts, touch at the specific EP. The two figures demonstrate the exotic topology of the eigenvalue surfaces near an EP singularity: for the real part, the two bands cross each other on one side of the EP and repel each other on the other side; while for the imaginary part, opposite occurs, where the crossing of the real (imaginary) part is accompanied by the repulsion of the imaginary (real) part. Figures 2(c) and 2(d) illustrate the projections of the eigenvalues onto the (k_x, ω) plane and (k_x, γ) plane, respectively, offering a clearer description of the transition from repulsion to crossing in the real and imaginary parts as k_x increases. The critical point of the transition exactly corresponds to the EP.

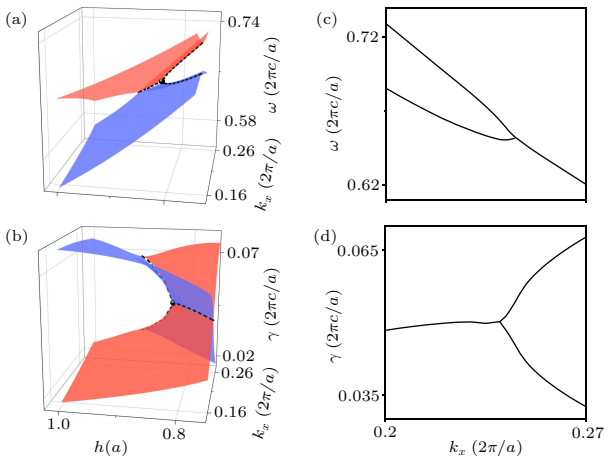


Fig. 2. EPs generated by coupling $\text{FP}_{\text{TM},3}$ and $\text{GR}^{(-1)}_{\text{TM},1}$ modes in parameter space. Panels (a) and (b) illustrate, respectively, the real part and imaginary parts of the eigenvalues, where the red surface and the blue surface correspond to the upper band and the lower band, respectively. The black dash lines indicate the crossing section determined by the intersection lines of the two sheets in the real and imaginary parts, and black spheres represent the EP. (c) and (d) The projections of the dash lines in (a) and (b), respectively. Here the parameters for the PhC slab are $\varepsilon_1 = 5.5$, $\varepsilon_2 = 2$, $h = 1.4a$, and $d = 0.5a$.

Next, we consider the coupling of the FP and GR modes with different polarizations. The two modes cannot couple with each other on the k_x axis due to the polarization orthogonality; however, away from the k_x axis, they are not orthogonal and coupling can occur. We calculate the coupling of the $\text{FP}_{\text{TM},2}$ and $\text{GR}^{(-1)}_{\text{TE},1}$ modes using the finite element method,

and the dispersions are shown in Figs. 3(a) and 3(b) for the real and imaginary parts, respectively. From Fig. 3(a) one can see that the upper band and lower band touch along a curve segment (the black dash line). For the imaginary part shown in Fig. 3(b), the opposite happens: the repulsion and crossing of the two sheets for the imaginary parts correspond to the crossing and repulsion of the real parts, respectively. There are two points at which both the real part and the imaginary part of the eigenvalues coalesce, forming two EPs. The curve segment connecting the two EPs in Fig. 3(a) is the so called Fermi arc.[33,36] In the reported work,[33] the EP pairs and the connecting Fermi arc are achieved as follows: first, a quadratic degeneracy point at the Γ point of a PhC splits into a pair of Dirac points by breaking the C_{4v} symmetry, then the PhC is reduced into a PhC slab which turns the Hermitian system into a non-Hermitian system. As a result, the original Dirac points break into EP pairs connected by the isofrequency line segment, that is, the Fermi arc.

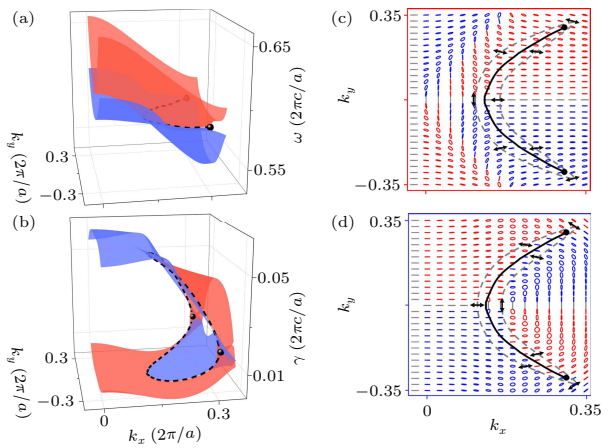


Fig. 3. EP pairs and Fermi arc generated from the coupling of $\mathrm{FP}_{\mathrm{TM},2}$ and $\mathrm{GR}^{(-1)}_{\mathrm{TE},1}$ modes. Here the parameters of the PhC slab are set as $\varepsilon_1 = 5.5$, $\varepsilon_2 = 1$, $h = 1.4a$, $d = 0.5a$. The real part and imaginary part of the eigenvalues are presented in (a) and (b), respectively. The red surface corresponds to the upper band and the blue surface corresponds to the lower band. The black dash lines indicate the Fermi arc, and the two black dots indicate the EPs. (c) and (d) The far-field polarization patterns of the upper band and lower band, respectively. The polarization states are illustrated by the ellipses, with red color and blue color representing the right-handed and left-handed elliptical polarizations. The Fermi arcs and EPs are indicated by the black solid lines and black dots, respectively. Gray arrows on the gray contours encircling the EP pair and the Fermi arc indicate the polarization directions (the long axis of the ellipses). The evolution of the polarization orientation along the contour manifests a topological charge of $-1/2$.

The far-field polarization patterns of the two bands are displayed in Figs. 3(c) and 3(d). For convenience, the two EPs and the Fermi arcs are plotted as well. Due to the mirror symmetry of the system, the dispersion and the corresponding far field polarization exhibit the same symmetry. Meanwhile, the far field polarization of the two bands formed by the mode coupling carries the polarization characteristics of the original $\mathrm{FP}_{\mathrm{TM},2}$ and $\mathrm{GR}^{(-1)}_{\mathrm{TE},1}$ modes. For example, the polarizations on the left side of the Fermi arc in Fig. 3(c) and that on the right side of the Fermi arc in Fig. 3(d) correspond to the polarization of the $\mathrm{GR}^{(-1)}_{\mathrm{TE},1}$ mode; and the polarizations on the left side of the Fermi arc in Fig. 3(d) and that on the right side of the Fermi arc in Fig. 3(c) correspond to the polarization of the $\mathrm{FP}_{\mathrm{TM},2}$ mode. This can be identified by examining the polarization on the k_x axis.

The peculiar topology of the band structure near the EPs and Fermi arc leads to nontrivial topological property,[33] which can be manifested by the corresponding far field polarization distribution. As shown in Figs. 3(c) and 3(d), along the gray curves surrounding the Fermi arcs and EPs, the orientation of the long axis of the polarization ellipses undergoes a 180° clockwise turn, indicating a topological charge of $-1/2$, consistent with that in the reported works.[33,36]

4. Conclusion and perspectives

In this paper, we show that FP modes in PhC slabs are not merely background fields but genuine EM modes characterized by their resonance nature. First we establish that the transmittance of a PhC slab can be viewed as the coupling of FP modes with the incoming and outgoing waves, thereby showcasing FP modes as authentic modes. Next, we utilize the coupling of FP mode with GR mode to achieve EP in PhC slabs, and a Fermi arc is also observed. The nontrivial topology of the Fermi arc and the EP pair is evidenced by the corresponding far field polarization pattern, which carries a topological charge of $-1/2$.

As widespread modes in PhC slabs, FP modes can offer abundant opportunities for mode coupling in addition to the GR–GR coupling, thus enriching the methods of optical field regulation.

Acknowledgment

Project supported by the National Natural Science Foundation of China (Grant Nos. 12074049 and 12347101).

References

[1] Saleh B E A, Teich M C 2007 *Fundamentals of Photonics* 2nd edn. (New Jersy: John Wiley & Sons, Inc. Hoboken) pp. 243–288
[2] Gellineau A, Yu-Po Wong and Solgaard O 2014 2014 *International Conference on Optical MEMS and Nanophotonics*, August 17–21, 2014, Glasgow, UK, p. 57
[3] Gellineau A, Wong Y P and Solgaard O 2013 *Opt. Lett.* **38** 4992
[4] Fan S and Joannopoulos J D 2002 *Phys. Rev. B* **65** 235112
[5] Joannopoulos J D, John S G, Winn J N and Meade R D 2008 *Photonic Crystals: Molding the Flow of Light*, 2nd edn. (New Jersy: Princeton University Press) pp. 44–65
[6] Zhang Z, Wang F, Wang H, Hu Y, Yin X, Hu W and Peng C 2022 *Opt. Lett.* **47** 2875
[7] Zhou H, Zhen B, Hsu C W, Miller O D, Johnson S G, Joannopoulos J D and Soljačić M 2016 *Optica* **3** 1079
[8] Hsu C W, Zhen B, Lee J, Chua S L, Johnson S G, Joannopoulos J D and Soljačić M 2013 *Nature* **499** 188

[9] Kang M, Zhang S, Xiao M and Xu H 2021 *Phys. Rev. Lett.* **126** 117402

[10] Cerjan A, Hsu C W and Rechtsman M C 2019 *Phys. Rev. Lett.* **123** 023902

[11] Hsu C W, Zhen B, Stone A D, Joannopoulos J D and Soljačić M 2016 *Nat. Rev. Mater.* **1** 16048

[12] Bulgakov E N and Sadreev A F 2008 *Phys. Rev. B* **78** 075105

[13] Hu P, Wang J, Jiang Q, Wang J, Shi L, Han D, Zhang Z Q, Chan C T and Zi J 2022 *Optica* **9** 1353

[14] Heiss W D 2012 *J. Phys. A: Math. Theor.* **45** 444016

[15] Miri M A and Alù A 2019 *Science* **363** eaar7709

[16] Lin Z, Ramezani H, Eichelkraut T, Kottos T, Cao H and Christodoulides D N 2011 *Phys. Rev. Lett.* **106** 213901

[17] Hassan A U, Galmiche G L, Harari G, LiKamWa P, Khajavikhan M, Segev M and Christodoulides D N 2017 *Phys. Rev. A* **96** 052129

[18] Wang C, Jiang X, Zhao G, Zhang M, Hsu C W, Peng B, Stone A D, Jiang L and Yang L 2020 *Nat. Phys.* **16** 334

[19] Hodaei H, Hassan A U, Wittek S, Garcia-Gracia H, El-Ganainy R, Christodoulides D N and Khajavikhan M 2017 *Nature* **548** 187

[20] Chen W, Kaya Özdemir Ş, Zhao G, Wiersig J and Yang L 2017 *Nature* **548** 192

[21] Bai K, Fang L, Liu T R, Li J Z, Wan D and Xiao M 2023 *Nat. Sci. Rev.* **10** nwac259

[22] Hodaei H, Miri M A, Heinrich M, Christodoulides D N and Khajavikhan M 2014 *Science* **346** 975

[23] Feng L, Wong Z J, Ma R M, Wang Y and Zhang X 2014 *Science* **346** 972

[24] Xu H, Mason D, Jiang L and Harris J G E 2016 *Nature* **537** 80

[25] Doppler J, Mailybaev A A, Böhm J, Kuhl U, Girschik A, Libisch F, Milburn T J, Rabl P, Moiseyev N and Rotter S 2016 *Nature* **537** 76

[26] Hassan A U, Zhen B, Soljačić M, Khajavikhan M and Christodoulides D N 2017 *Phys. Rev. Lett.* **118** 093002

[27] Ghosh S N and Chong Y D 2016 *Sci. Rep.* **6** 19837

[28] Zhen B, Hsu C W, Igarashi Y, Lu L, Kaminer I, Pick A, Chua S L, Joannopoulos J D and Soljačić M 2015 *Nature* **525** 354

[29] Yin X, Inoue T, Peng C and Noda S 2023 *Phys. Rev. Lett.* **130** 056401

[30] Luo L, Shao Y, Li J, Fan R, Peng R, Wang M, Luo J and Lai Y 2021 *Opt. Express* **29** 14345

[31] Kamiński P M, Taghizadeh A, Breinbjerg O, Mørk J and Arslanagić S 2017 *Opt. Lett.* **42** 2866

[32] Wonjoo Suh, Zheng Wang, and Shanhui Fan 2004 *IEEE J. Quantum Electron.* **40** 1511

[33] Zhou H, Peng C, Yoon Y, Hsu C W, Nelson K A, Fu L, Joannopoulos J D, Soljačić M and Zhen B 2018 *Science* **359** 1009

[34] Ping S 2006 *Introduction to Wave Scattering, Localization and Mesoscopic Phenomena* 2nd edn. (Berlin: Springer Berlin Heidelberg) pp. 45–116

[35] Özdemir Ş K, Rotter S, Nori F and Yang L 2019 *Nat. Mater.* **18** 783

[36] Chen W, Yang Q, Chen Y and Liu W 2021 *Proc. Natl. Acad. Sci. USA* **118** e2019578118